Table Of Contents

Submissions

ERCOFTAC Bulletin
Institute of Thermal Machinery
Częstochowa University of Technology
Al. Armii Krajowej 21
42-201 Częstochowa
Poland
Tel: +48 343 250 507
Fax: +48 343 250 507
Email:ercoftac@imc.pcz.czest.pl

Hosted, Printed & Distributed By

Częstochowa University of Technology

ISSN: 2518-0991

Next *ERCOFTAC* Events

ERCOFTAC Spring Festival
6th April, 2017
Vienna, Austria

ERCOFTAC Committee Meetings
6th April, 2017, 2016
Vienna, Austria

European Research Community on Flow, Turbulence and Combustion

ERCOFTAC is a leading European association of research, education and industry groups in the technology of flow, turbulence and combustion. The main objectives of *ERCOFTAC* are: To promote joint efforts of European research institutes and industries with the aim of **exchanging technical and scientific information**; to promote **Pilot Centres** for collaboration, stimulation and application of research across Europe; to stimulate, through the creation of **Special Interest Groups**, wellcoordinated European-wide research efforts on specific topics; to stimulate the creation of advanced training activities; and to be influential on funding agencies, governments, the European Commission and the European Parliament.

www.ercoftac.org

Prediction of Bypass and Separation-Induced Transition With an Algebraic Intermittency Model

S. Kubacki[1], T. Borzecki[2], E. Dick[3]

[1] *Institute of Aeronautics and Applied Mechanics, Warsaw University of Technology, Nowowiejska 24, 00-665, Warsaw, Poland*

[2] *Avio Aero, Grazynskiego 141, 43-300 Bielsko-Biala*

[3] *Department of Flow, Heat and Combustion Mechanics, Ghent University, St.-Pietersnieuwstraat 41, 9000 Ghent, Belgium*

Slawomir.Kubacki@meil.pw.edu.pl

Abstract

The paper discusses applications of an algebraic intermittency model for prediction of bypass and separation-induced boundary layer transition. The transition model is coupled with a $k-\omega$ turbulence model. The transition model uses only local variables and is tuned for turbomachinery flows. For bypass transition, two effects in an attached pre-transitional boundary layer are modelled: damping of small-scale disturbances induced by the free stream and breakdown of the near-wall perturbed flow with generation of fine-scale turbulence. For separated flow, the model describes breakdown of a laminar free shear layer. We refer to [1] for a complete discussion of the modelling assumptions and the model validation.

1 Transition mechanisms

Transition mechanisms in an attached laminar boundary layer subjected to a high free-stream turbulence level (above 0.5-1%) are discussed by Hack and Zaki [2]. Streamwise elongated disturbances are generated. These are zones of forward and backward jet-like perturbations, alternating in spanwise direction. They are called streaks or Klebanoff disturbances. Streaks grow downstream both in length and amplitude and finally some streaks cause turbulent spots. Transition is then called of bypass type, which means that instability by Tollmien-Schlichting waves is bypassed. Breakdown is then earlier and much faster. Klebanoff modes are initiated by deep penetration into a laminar boundary layer of large-scale perturbations from the free stream. The strong damping of small-scale components is called shear sheltering. There are at least two instability mechanisms in a boundary layer perturbed by streaks. One is instability by inflection of the velocity profile in wall-normal direction between the boundary layer edge and a low-speed streak. The other is instability of the velocity profile in wall-normal direction in the overlap zone of the leading edge of a high-speed streak and the trailing edge of a low-speed streak. Both instabilities are triggered by small-scale perturbations, although these are damped in the boundary layer

Transition mechanisms in a separated laminar boundary layer are discussed by McAuliffe and Yaras [3]. Under low free-stream turbulence, transition is initiated by inviscid Kelvin-Helmholtz instability, with formation of spanwise vortices. They group at selective streamwise wavelengths, analogous to Tollmien-Schlichting waves in an attached boundary layer. The roll-up vortices break down as they travel downstream. The breakdown process is rather slow with low free-stream turbulence, but, under high free-stream turbulence, bypass transition with formation of streaks in the attached boundary layer prior to separation can co-exist with the Kelvin-Helmholtz generated spanwise vortices in the separated layer. The breakdown of the vortex rolls is then strongly accelerated by perturbations due to the Klebanoff modes. For sufficiently strong free-stream turbulence, the Kelvin-Helmholtz instability may even be bypassed by the breakdown of the streaks. So, a bypass mechanism is possible in a separated shear layer, similar as in an attached boundary layer.

2 Model formulation

The transport equations for turbulent kinetic energy and specific dissipation read

$$\frac{Dk}{Dt} = \gamma P_k + (1-\gamma)P_{sep} - \beta^* k\omega + Diff(k) \quad (1)$$

$$\frac{D\omega}{Dt} = \alpha\frac{\omega}{k}P_k - \beta\omega^2 + Diff(\omega) \quad (2)$$

The basic equations are the $k-\omega$ equations of the turbulence model of Wilcox [4], but there are three modifications in the production terms. In the original model, production of turbulent kinetic energy by turbulent shear is $P_k = \nu_T S^2$, with ν_T the full eddy viscosity and $S = (2S_{ij}S_{ij})^{1/2}$ the magnitude of the shear rate tensor. Firstly, this production term is written as $P_k = \nu_s S^2$, where ν_s is the small-scale eddy viscosity, which is part of the full eddy viscosity ν_T. Secondly, the production term P_k is multiplied with an intermittency factor γ which is zero in laminar flow and unity in turbulent flow. Thirdly, the term $(1-\gamma)P_{sep}$ is added to the production term of the k-equation. This term models turbulence production by instability and breakdown of a laminar free shear layer in a low turbulence level background flow.

The turbulent kinetic energy k is split, based on the laminar-fluctuation kinetic energy transition model of Walters and Cokljat [5], into a small-scale part and a large-scale part:

$$k_s = f_{SS}k, \quad k_l = k - k_s \quad (3)$$

The splitting by the factor f_{SS} expresses the shear-sheltering effect in a pre-transitional boundary layer. Small-scale disturbances in the turbulent flow near to the

laminar part of the layer are damped. Only large-scale disturbances penetrate deeply into the laminar layer, but these do not contribute to turbulence production by shear but induce the streaks. The restriction of the turbulence production by turbulent shear to small-scale fluctuations is expressed by replacing the full eddy viscosity by a small-scale eddy viscosity in the production terms of the $k-$ and $\omega-$equations (Eqs. 1 and 2).

Shear-sheltering depends on the ratio of two timescales in a laminar layer: the timescale of convection of disturbances relative to an observer inside the layer and the timescale of diffusion in the normal direction. Walters [6] estimates the convective time scale by the time scale of the strain, $\tau_c = 1/\Omega$, with Ω the magnitude of the vorticity tensor. The diffusive time scale in a laminar layer is fundamentally l^2/ν, with l the fluctuation length scale in normal direction and ν the kinematic fluid viscosity. Walters [6] expresses damping of small-scale fluctuations in a pre-transitional boundary layer by stating that fluctuations in the border zone of the laminar and turbulent parts synchronise strongly with the mean velocity gradient in the laminar part. So, he assumes that fluctuations, both in streamwise and in wall-normal direction, after damping, scale with $l\Omega$. This means proportionality between $\sqrt{k}$ and $l\Omega$, resulting in $l \propto \sqrt{k}/\Omega$ and $\tau_d \propto k/(\nu\Omega^2)$. The ratio of the diffusive and convective timescales is the Reynolds number $Re_\Omega = k/(\nu\Omega)$.

With the supplementary assumption that in the laminar part of a pre-transitional boundary layer the wall-normal fluctuation length scale is proportional to the distance to the wall, denoted by y,Ω may be eliminated by replacing it by $\sqrt{k}/y$. This means that the characteristic Reynolds number for shear-sheltering may also be $Re_y = \sqrt{k}y/\nu$. We use the shear-sheltering factor of Walters and Cokljat [5], but replace Re_Ω by Re_y,leading to

$$f_{SS} = exp\left(-\left(\frac{C_{SS}\nu}{\sqrt{k}y}\right)^2\right) \tag{4}$$

$C_{SS} = C_S(1 + C_A f_W \Psi)$ is a flow-dependent coefficient. C_S and C_A are constants (Table 1). C_A is set to unity while C_S has been determined by simulations of T3C flat plate flows of ERCOFTAC (not disused here). The Ψ and f_W functions are:

$$\Psi = tanh\left(\frac{-\Omega(S-\Omega)}{C_\Psi(\beta^*\omega)^2}\right),\ f_W = 1 - tanh\left(\frac{k}{C_W\nu\omega}\right) \tag{5}$$

The role of the flow-dependent term $f_W\Psi$ is increasing C_{SS} (larger shear sheltering) in accelerating flow ($f_W\Psi > 0$), and reducing C_{SS} (smaller shear sheltering) in decelerating flow ($f_W\Psi < 0$), due to streamline curvature. The Ψ function is the curvature sensor from the non- linear eddy-viscosity turbulence model of Khodak and Hirsch [7]. The f_W function limits the correction to the border zone between laminar and turbulent parts in a pre-transitional boundary layer. The C_W and C_Ψ are positive constants, determined by simulations of flows through the N3-60 steam turbine cascade and the V103 compressor cascade. We discuss simulations of the N3-60 cascade later.

The eddy viscosity associated to small scales is calculated in the same way as the eddy viscosity of the original turbulence model [4] by replacing k by k_s:

$$\nu_s = \frac{k_s}{\tilde{\omega}}, with\ \tilde{\omega} = max\left[\omega, \frac{C_{lim}S}{a_s}\right] \tag{6}$$

The constant a_s is set to 0.3 and $C_{lim} = 7/8$, which are the standard values. The large-scale eddy viscosity, is, similarly defined with k_l:

$$\nu_l = \frac{k_l}{\tilde{\omega}}, with\ \tilde{\omega} = max\left[\omega, \frac{C_{lim}S}{a_l}\right] \tag{7}$$

The constant a_l is set to 0.6, which is larger than the standard value 0.3. The resulting eddy viscosity, used in the Navier-Stokes equations, is $\nu_T = \nu_s + \nu_l$. The reason for the enlarged value of a_l with respect to a_s is earlier transition due to increased instability of a laminar flow perturbed by streaks under an adverse pressure gradient. The values of the a_l and C_W constants (Table 1) have been modified somewhat with respect to the values used in [1]. This change is the result of further model calibration on an extended number of cases.

The intermittency function γ determines when a flow region is laminar or turbulent. The free stream is turbulent. Thus γ is set to unity in the free stream. At a wall, the flow is laminar. Hence, γ is set to zero there. γ is prescribed algebraically as a function of the distance to the wall by

$$\gamma = min\left(max\left(\frac{\sqrt{k}y}{A_\gamma\nu} - 1, 0\right), 1\right) \tag{8}$$

were A_γ is a constant.

The motivation for $Re_y = \sqrt{k}y/\nu$ as non-dimensional distance to the wall (Eq. 8) originates from the work of Wang et al. [11], who observed that breakdown occurs when, near to the wall, the ratio of turbulent shear stress to wall shear stress reaches a critical value. Near to a wall, the streamwise fluctuation u' in a pre-transitional boundary layer is caused by streaks. So, we may assume that near to a wall u' scales with $y\Omega$. Near to a wall, urbulent kinetic energy is strongly damped and with a turbulence model $\sqrt{k}$ becomes representative for v'. So, the near-wall turbulent shear stress, obtained by multiplying u' by the wall-normal fluctuation v' and time-averaging, can be estimated by $-\rho < u'v' > \propto \rho y\Omega\sqrt{k}$ The wall shear stress is $\tau_w = \rho\nu\Omega_w$. So, the ratio of both terms gives the characteristic Reynolds number $Re_y = \sqrt{k}y/\nu$.

The intermittency function is somewhat simplified with respect to the function of our previous work [8] by equalising the threshold value C_T and the growth rate A_T ($C_T = A_T = A_\gamma$), but this is not a significant change. A more significant change concerns the shear-sheltering factor (Eq. 4). We used the factor from the model by [5] with Re_Ω as input parameter in our previous work [8]. In [1] we replaced Re_Ω by Re_y , such that f_{SS} is now also dependent on the distance to the wall, normalised in the same way as in the intermittency function. This change improves much the correspondence between predictions of the onset of transition by the model and empirical correlations (improved results are not shown here; consult Figs. 8 and 9 in [8] for previous results and Figs. 9 and 10 in [1] for new results).

The present model, in contrast to our previous version, includes turbulence production due to breakdown of a laminar separated boundary layer at low free-stream turbulence level using 2D RANS (or 2D/3D URANS). This is realised by the term $(1-\gamma)P_{sep}$ in the $k-$ equation (Eq. 1). For, P_{sep} we adopt a term with the same purpose in the newest intermittency-transport transition model by Menter et al. [9]:

$$P_{sep} = C_{sep}F_{sep}\nu S^2 \tag{9}$$

$$F_{sep} = min\left(max\left(\frac{R_V}{2.2A_V} - 1, 0\right), 1\right) \tag{10}$$

Table 1: Transition model constants

A_γ	C_S	C_A	C_Ψ	C_W	C_{sep}	A_V	a_1
12.0	21.0	1.0	10.0	10.0	2.0	550.0	0.6

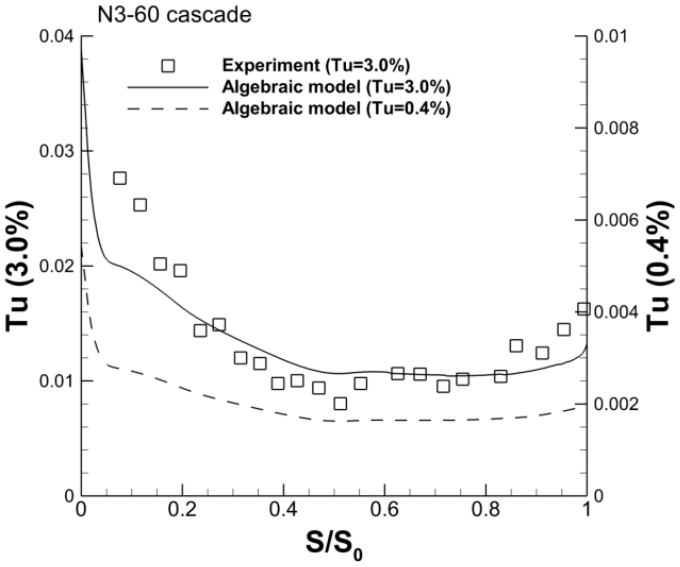

Figure 1: N3-60 cascade. Turbulence intensity along the suction side of the blade at distance 10 mm from the blade surface for $Tu = 3\%$ and $Tu = 0.4$ %. S_0 is the length of the suction side of the blade

with $R_V = y^2 S/\nu$. The constants C_{sep} and A_V have been calibrated for the T3C4 flat plate flow of ERCOFTAC, which is characterized by laminar boundary layer separation in the rear part of the plate (result are not shown). Table 1 lists the model constants.

3 Computational aspects

All simulations reported here are for the N3-60 steam turbine cascade using 2D RANS or 2D URANS. The 2D computational grids, with about $1.1 \cdot 10^5$ cells, consist of a structured boundary layer part with quadrilateral cells near to walls and an unstructured part away from walls. The grid is refined near to walls. The y^+ parameter varies between 0.1 and 0.8 along walls and about 40 cells are used across the boundary layer grid part.

4 N3-60 cascade with steady inflow

We discuss the model performance for transition in attached and in laminar separation states by 2D RANS for steady inflow of the N3-60 cascade, measured by Zarzycki and Elsner [10]. The N3-60 profile is the enlarged profile of a stator vane in the high-pressure part of a steam turbine. Geometric data are: blade chord 300 mm, axial blade chord 203.65 mm, blade pitch 240 mm. The exit Reynolds number is $6 \cdot 10^5$. Measurements are available for inflow turbulence $Tu = 3\%$ and $Tu = 0.4\%$ in the leading edge plane. Laminar separation occurs at the suction side for $Tu = 0.4\%$

At the inlet to the computational domain, placed at 0.344 times the axial chord length upstream of the leading edge, a uniform flow velocity in the axial direction was imposed. The inlet turbulence intensity in the leading edge plane was set according to the two sets of experimental data. The inlet turbulent length scale was not reported in the measurements. For $Tu = 3$ %, the inlet turbulent length scale was adjusted by matching the measured turbulence intensity at a distance of 10 mm from the blade surface (this is above the boundary layer edge). The obtained turbulent length scale is $l_t = 6$ mm for $Tu = 3$ %. Fig. 1 shows that the agreement between prediction and measurement is reasonably good, which means that the inlet conditions for the modelled scalars have been set correctly. For low turbulence level at inlet ($Tu = 0.4\%$), the evolution of the free-stream turbulence along the blade surface is not available in the database. We assume a smaller length scale ($l_t = 2$mm) at the entrance to the cascade than for high inlet turbulence level since no turbulence grid was installed in the reference experiment. The turbulent intensity reproduced at the leading edge of the blade corresponds with measurements, $Tu = 0.5$-0.4% (Fig. 1).

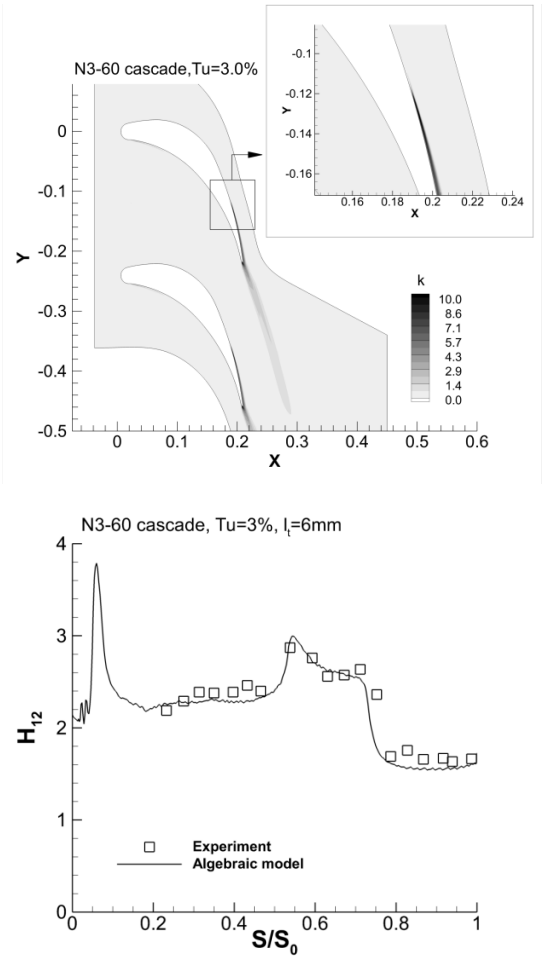

Figure 2: N3-60, Tu = 3%. Turbulent kinetic energy (top) and shape factor along the suction side of the blade (bottom) using 2D RANS

Fig. 2 shows the contour plot of turbulent kinetic energy for $Tu = 3\%$ and the comparison between computed and measured shape factor H_{12} along the suction side of the blade. The simulated transition comes from the bypass term γP_k in Eq. 1. Transition onset, at $S/S_0 = 0.75$, and growth rate in the transition zone are reproduced correctly by the model.

Fig. 3 shows the contour plot of turbulent kinetic energy for $Tu = 0.4\%$ and the comparison between com-

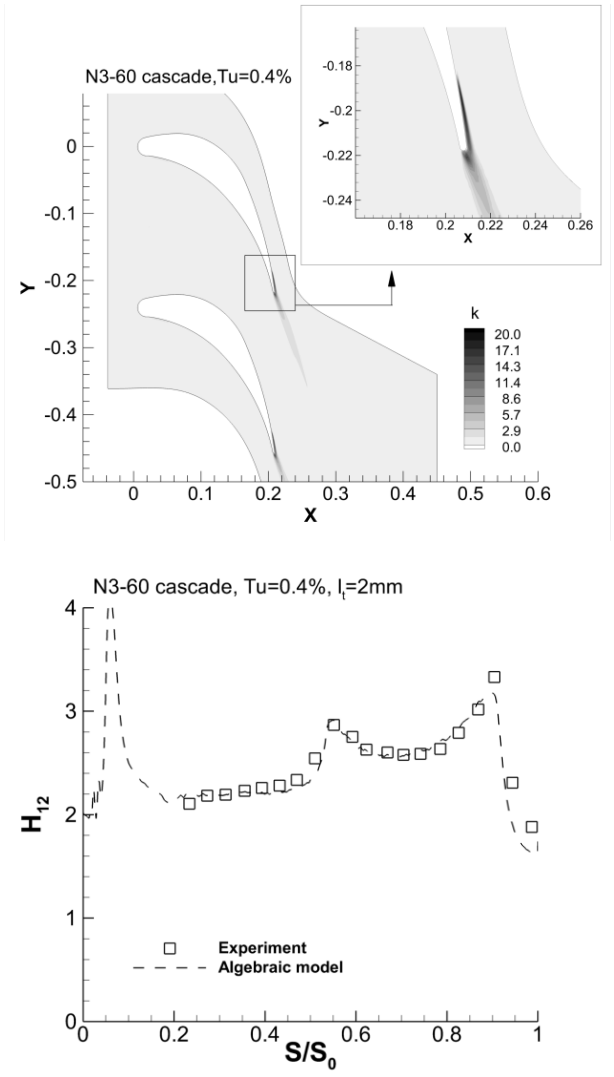

Figure 3: N3-60, $Tu = 0.4\%$. Turbulent kinetic energy (top) and shape factor along the suction side of the blade (bottom) using 2D RANS

puted and measured shape factor H_{12} along the suction side of the blade. The simulated transition comes here from the separation term $(1-\gamma)P_{sep}$ in Eq. 1. Start of transition is observed at $S/S_0 = 0.9$. The agreement between simulation and measurement is good. It means that the model calibration for separation-induced transition by the T3C4 case has been done well. We bring to the attention that in the previous model [8] the transition in a separated laminar boundary layer was not modelled, but was resolved using 3D URANS. This is no longer necessary, as transition in a separated boundary layer is fully modelled now [1].

5 N3-60 cascade with unsteady inflow

The final model validation is performed with wake- induced transition for flow through the N3-60 cascade using 2D URANS. Simulation results are compared with measurements by Zarzycki and Elsner [10]. In the experiments the wake generator was a wheel of pitch diameter $D_p = 1950$ mm with cylindrical bars rotating in a plane perpendicular to the flow direction. The bars were spaced by b_s= 204 mm on the pitch circle. The axial distance between the bars and the leading edge of the blades was 0.344 of the axial blade chord. The frequency of the incoming wakes was $f_d = 59$ Hz, with inflow velocity $U_0 = 10$ m/s, resulting in the reduced frequency: $S_t = f_d b_s/U_0 = 1.22$. The exit Reynolds number was $6 \cdot 10^5$. The free-stream turbulence intensity Tu was controlled with a movable grid upstream of the cascade entrance. We use the data for bar diameters d=6 and 4 mm with inflow turbulence levels $Tu = 3$ and 0.4 %, respectively. The inlet to the computational domain is placed at 0.17 times the axial chord length upstream of the leading edge. The effect of the moving bars was superimposed on the flow obtained from the steady calculation. The bar pitch has been increased to 240 mm to be equal to the blade pitch in the calculation. The bar velocity has been adjusted, so that the reduced frequency (St) of the impacting wakes is unchanged. 800 time steps were used per wake period. Self-similar profiles for velocity and turbulent kinetic energy were imposed at the inlet:

$$U = U_\infty - (U_\infty - U_{center}) exp\left[-(ln2)\left(\frac{y}{y_{1/2}}\right)^2\right],$$
$$k = k_\infty + (k_{center} - k_\infty) exp\left[-(ln2)\left(\frac{y}{y_{1/2}}\right)^2\right] \quad (11)$$

In the above expressions, y is the distance perpendicular to the wake with $y = 0$ the centre of the wake and $y_{1/2}$ is the position where the defect of the velocity attains half of its maximum value. The parameters in the above expressions have been fitted to experimental data for wakes of stationary bars. The specific dissipation at the inlet was imposed following Wilcox [12]:

$$\omega = \omega_\infty + C_\mu^{1/4}\frac{\sqrt{k}}{l_{mix}}, l_{mix} = 0.18 y_{1/2} \quad (12)$$

The background dissipation ω_∞ has been used to adjust the evolution of the fluctuating velocity component parallel to the blade, $u' = (2k/3)^{1/2}$, at distance 10 mm from the suction surface of the blade to the experimental one for moving bars (results are not shown).

Fig. 4 shows the perturbation velocity vectors in every 15 cells. The perturbation velocity field is obtained by subtracting the time-averaged velocity field from the instantaneous velocity field. Clearly, the 1.1×10^5 mesh is sufficient to properly reproduce the negative jet effect caused by a moving wake.

Fig. 5 shows space-time diagrams of shape factor obtained in the experiment (a) and in the simulation (b) for wake-induced transition with background turbulence level $Tu = 3$ % (d = 6mm). The two straight lines mark the path of the moving wake. The wake position was determined from the free-stream velocity at the edge of the boundary layer. The bottom line is the path of the leading edge of the wake, determined as the position at which local flow acceleration starts in the rear part of the blade ($S/S_0 > 0.6$). The upper line corresponds to the central part of the moving wake, determined as the start of local flow deceleration.

The agreement between simulation and measurement is very good under the wake impact ($S/S_0 = 0.6$, $\tau/T = 0.2$). The width of the turbulent zone is somewhat too large at $S/S_0 = 0.7-0.8$ and the transition is reproduced somewhat too late in between wakes near to the trailing edge ($S/S_0 = 0.9$, $1.0 < \tau/T < 1.2$).

Fig. 6 shows space-time diagrams of shape factor for wake-induced transition with background turbulence

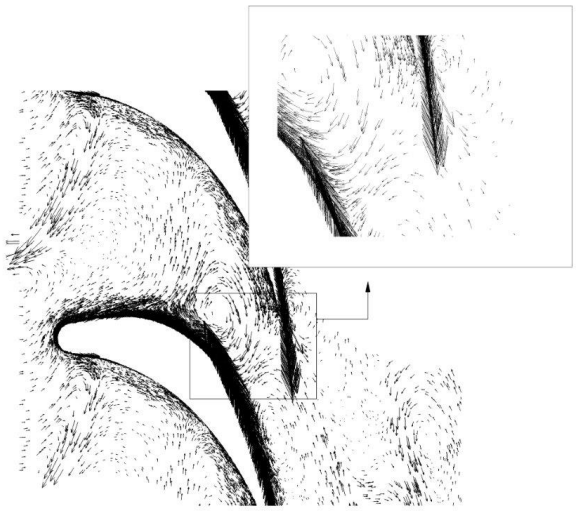

Figure 4: Negative jet visualised by perturbation velocity vectors in every 15 cells for 2D URANS

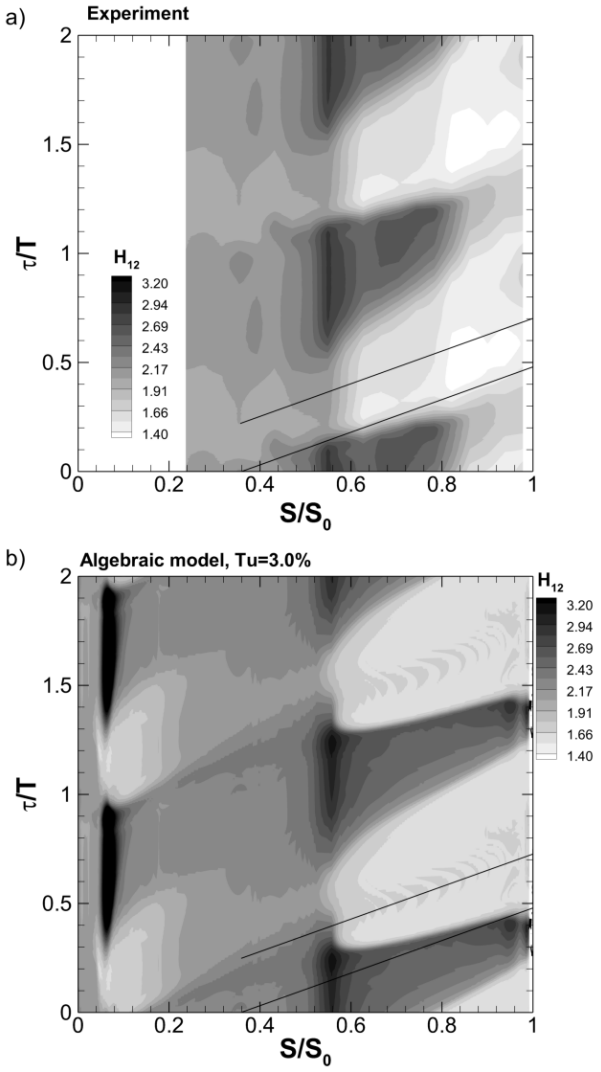

Figure 5: N3-60 cascade, bar diameter 6 mm and background turbulence level 3 %. Space-time diagrams of shape factor, a) experiment, b) simulation

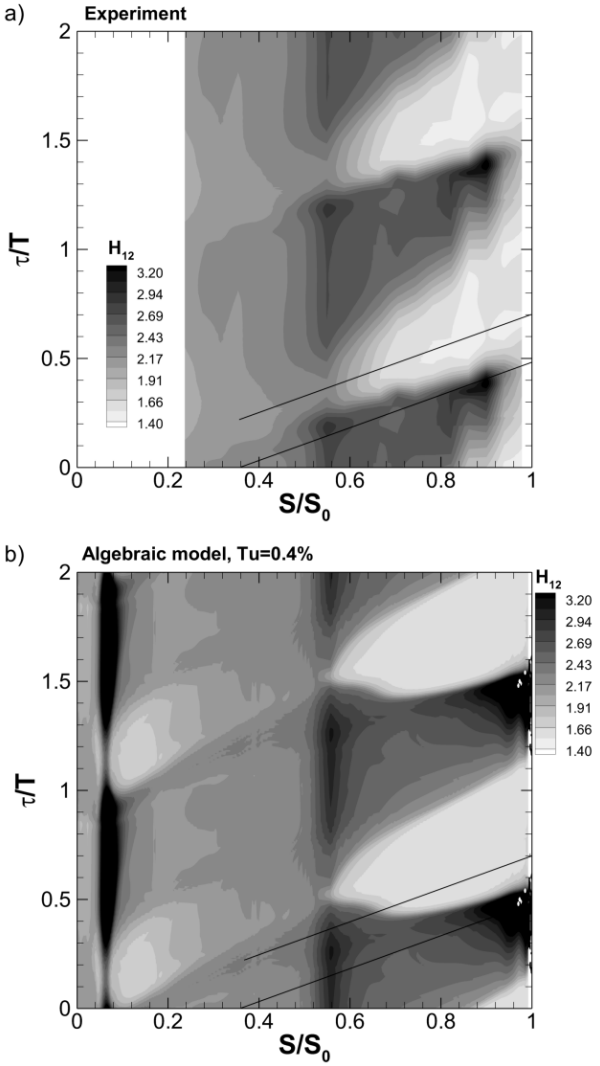

Figure 6: N3-60 cascade, bar diameter 4 mm and background turbulence level 0.4 %. Space-time diagrams of shape factor, a) experiment, b) simulation

level $Tu = 0.4$ % ($d = 4$mm). The model is able to properly detect transition onset under the wake impact ($S/S_0 = 0.7$,$\tau/T = 0.4$). The width of the turbulent zone, after wake impact, is comparable in both simulation and measurement. The quality of the model becomes less in between wakes ($S/S_0 = 0.9$, $1.1 < \tau/T < 1.5$) near to the trailing edge of the blade. The model predicts flow separation, which is not present in the experiment. The explanation is the somewhat too low free-stream turbulence level reproduced in the simulation in the rear part of the blade, which causes delayed transition there. In the experiment, interaction occurs near the suction side trailing edge between the wake of the adjacent blade and the moving wake through the blade passage. Vortices are shed from the blade wake, which beak down, causing increased free-stream turbulence. This interaction is not detected in the 2D URANS simulation.

Overall, the simulation results of wake-induced transition both at high ($Tu = 3\%$) and low ($Tu = 0.4\%$) background turbulence levels are good using the present algebraic transition model.

6 Conclusions

Applications of an algebraic intermittency model have been presented. The model produces good results for bypass and separation-induced transition (2D RANS) and for wake-induced transition (2D URANS), for flow through the stream turbine vane cascade N3-60, at both high and low free-stream turbulence levels.

Acknowledgement

The first and second author acknowledge support from the research project COOPERNIK financed partly by the Polish National Centre for Research and Development (INNOLOT/I/11/NCBR/2014) and partly by Avio Polska Sp. z o.o.

References

[1] Kubacki S., Dick E., An algebraic intermittency model for bypass, separation-induced and wake- induced transition. To appear in: Int. J. Heat and Fluid Flow (available online: doi: 10.1016/j.ijheatfluidflow.2016.09.013).

[2] Hack M.J.P., Zaki T.A., Streak instabilities in boundary layers beneath free-stream turbulence, J. Fluid Mech. 741, 280-315, 2014.

[3] McAuliffe B.R., Yaras M.I., Transition mechanisms in separation bubbles under low- and elevated freestream turbulence, J. Turbomachinery 132, 011004/1-10, 2010.

[4] Wilcox D.C., Formulation of the $k-\omega$ turbulence model revisited. AIAA J., 46, 2823-2837, 2008.

[5] Walters D.K., Cokljat D., A three-equation eddy-viscosity model for Reynolds-averaged Navier-Stokes simulations of transitional flow, J. Fluids Engineering 130, 2401/1-14, 2008.

[6] Walters. K., Physical interpretation of transition-sensitive RANS models employing the laminar kinetic energy concept, Ercoftac Bulletin 80, 67-76, 2009.

[7] Khodak A., Hirsch C., Second-order non-linear $k-\omega$ models with explicit effect of curvature and rotation, in Proceedings of Third ECCOMAS Computational Fluid Dynamics Conference, Paris, France, Wiley, ISBN 0471958514, 690-696, 1996.

[8] Kubacki S., Dick E., An algebraic model for bypass transition in turbomachinery boundary layer flows, Int. J. Heat and Fluid Flow, 58, 68-83, 2016.

[9] Menter F.R., Smirnov P.E., Liu T., Avancha R., A one-equation local correlation-based transition model, Flow Turbul. Combust. 95, 583-619, 2015.

[10] Zarzycki R., Elsner W., The effect of wake parameters on the transitional boundary layer on a turbine blade, IMechE Part A, J. Power and Energy, 219, 471-480, 2005.

[11] Wang T., Keller F.J., Zhou D., Flow and thermal structures in a transitional boundary layer. Exp. Therm. Fluid Sci. 12, 352-363, 1996.

[12] Wilcox D.C., Turbulence modelling for CFD. DCW Industries, Inc, 1993.